Letter

Bound states in the continuum based on controlling the phase difference in dielectric corrugated structures

Bo Yan [*], Siqi Zhang [*], Bing Zhang, and Xiangqian Jiang [†]
School of Physics, Harbin Institute of Technology, Harbin 150001, China

(Received 5 June 2023; revised 8 July 2024; accepted 16 July 2024; published 1 August 2024)

Bound states in the continuum (BICs) with an infinite quality factor (Q factor) and lifetime are demonstrated as far-field polarization singularities in momentum space. Unidirectional guided resonances (UGRs) are only a V point (vortex polarization singularity) in the upper or lower half space to block the radiation channel. In photonic systems, the evolution between BICs and UGRs can be achieved by adjusting the structure parameters. However, the coexistence of BICs and UGRs has not been realized so far. Here, we propose a dielectric corrugated structure and find that the far-field radiation of the structure can be controlled by changing the phase difference between the upper and lower surfaces. The coexistence of BICs and UGRs can be achieved at a specified phase difference. Interestingly, as the V points evolve with the phase difference, a high Q factor platform is realized. Our results provide a means to achieve the high Q factor platform and the coexistence of BICs and UGRs in momentum space, which promotes greatly the study of far-field radiation manipulation and high Q factor resonance.

DOI: 10.1103/PhysRevB.110.L081401

Introduction. Bound states in the continuum (BICs) are the nonradiating states of an open system with a spectrum embedded in the continuum of the radiating modes [1–6], which have an infinite lifetime and an infinite quality factor (Q factor) [7–14]. BICs have attracted considerable interest as they can boost electric field enhancement and have been employed in many applications, such as light-emitting devices [15], sensors [16,17], and enhanced nonlinear phenomena [18–21]. In the past few years, BICs have been constructed by various mechanisms such as symmetry mismatch [22–24], parity-time symmetry [25,26], environment engineering [27], and topological charge evolution [28–33]. BICs are mainly divided into symmetry-protected BICs and accidental BICs [33–38]. The symmetry-protected BICs are generated from a mismatch between the resonance mode and the radiative channel, which makes outward radiation impossible. As for accidental BICs, the accidental disappearance of coupling coefficients of radiation waves is due to the destructive interference effect of multiple radiation channels [4,30,31,39–50]. The existence of BICs breaks the coupling between resonant modes and all outward radiation channels compatible with a given frequency and momentum, providing an important way to enhance and extremely localize the light field [40,51–56].

The BICs in an optical system have been widely discussed since they were realized for the first time in 2008 [57]. Subwavelength dielectric nanostructures such as grating, photonic crystal slabs, and metasurfaces provide efficient ways to manipulate light through BICs [2,58–63]. As we know, the symmetry of structures affects strongly the light radiation. Yin *et al.* proposed a one-dimensional silicon grating assembled of rectangular bars [29]. Introducing an angle between the vertical direction and sidewall of the bars, the structure supports BICs when the angle is zero. When the sidewall is tilted from the vertical direction for a specific angle, the up-down mirror symmetry is broken and the BICs convert to unidirectional guided resonances (UGRs), radiating only towards one side of the grating. In contrast, for a double-layer structure consisting of two identical one-dimensional silicon gratings with misalignment, the dynamics of topological polarization singularity and synthetic topological nodal phase have been studied [31,64]. The misalignment breaks the up-down mirror symmetry and C_2 symmetry, leading to high-contrast directional radiation and BICs. We noted that the evolution from BICs to UGRs can be achieved in momentum space via adjusting the angles of sidewall or misalignment of double-layer grating, however, the coexistence of BICs and UGRs still is a challenge.

In this Letter, we propose a silicon corrugated structure, and introduce the phase difference between the upper and lower surfaces. Different varieties of BIC points were obtained at phase differences with different symmetries. We simultaneously study the properties of far-field radiation in the upper and lower half spaces of topological polarization singularities, and observe the coexistence of BIC and UGRs. Moreover, by tuning the phase difference, the V points associated with BICs and UGRs can be alternatively distributed, which generates a uniform high Q factor platform. Our results provide a means to achieve the high Q factor platform and the coexistence of BICs and UGRs in momentum space.

Results and discussion. Figure 1(a) shows schematically the structure of the dielectric corrugated grating surrounded by air. The refractive index of the dielectric is $n = 3.53$, and the thickness of the grating is $h = 2000$ nm. The upper and lower surfaces can be given by $z_1(x) = A\sin(kx + \varphi)$ and $z_2(x) = A\sin(kx)$, respectively. Here, $k = 2\pi/a$ is the grating vector (with lattice constant $a = 3000$ nm), and $A = 300$ nm

[*]These authors contributed equally to this work.
[†]Contact author: xqjiang@hit.edu.cn

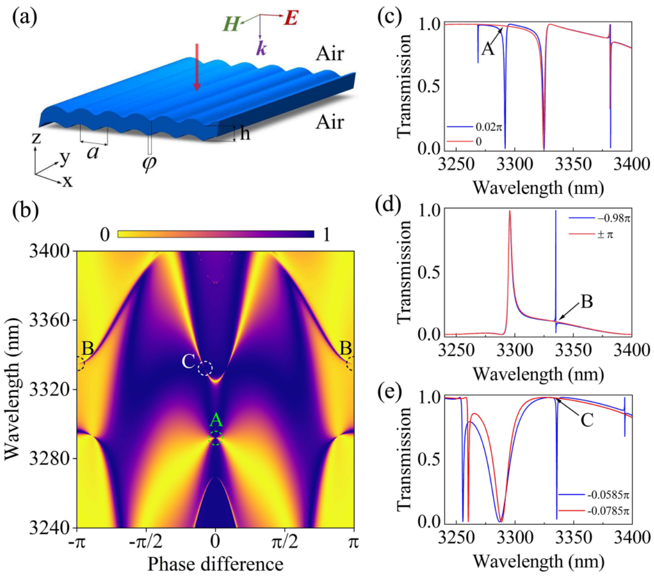

FIG. 1. BIC formation in the dielectric corrugated grating. (a) Schematic diagram of the dielectric corrugated grating under investigation. (b) Transmission spectrum of the dielectric corrugated as a function of the phase difference φ between the upper and lower surface at the normal incidence. The A and B points indicate two symmetry-protected BICs at the phase difference of 0 and $\pm\pi$, respectively. The C point indicates the accidental BIC at phase difference of $\varphi = -0.0785\pi$. The transmission coefficient of a dielectric corrugated structure with the phase difference between the upper and lower surface of (c) 0.02π and 0 (d) -0.98π and $\pm\pi$ (e) -0.0585π and -0.0785π, where black arrows point from collapse with sharp Fano line-shape resonances to BICs.

represents the amplitude of the grating. In the simulation, we hold the lower surface still and move the upper surface to change the phase differences between the upper and lower surfaces. The schematics of the structure with a phase difference are shown in Fig. 1(a). When $\varphi = 0$ the structure shows C_2 symmetry. The structure is of C_2 and up-down mirror symmetry when $\varphi = \pm\pi$. For the general case, the structure has an inversion symmetry (P symmetry). The simulation of the transmission property of the structure was accomplished by numerically solving Maxwell's equation using a finite-element method. Perfectly matched layers (PMLs) in the z direction and Floquet periodic boundary conditions in the x direction are used.

The transmission spectrum as a function of the phase difference φ between the upper and lower surfaces is shown in Fig. 1(b). There are a few discontinuous points in the spectrum. We can get high transmission at the breakpoints A and C, and when the phase difference deviates from the breakpoints, ultranarrow transmission peaks appear. Breakpoint B corresponds to a lower transmission, and the deviation from the breakpoints leads to ultranarrow transmission peaks. The symmetry-protected BICs (A, B) and the accidental BIC (C) are shown in Fig. 1(b), inside the green, black, and white dotted circles. In order to get the spectral line of the BIC point characteristics under a specified phase difference, the transmission spectra at phase differences $\varphi = 0$ and $\varphi = 0.02\pi$ ($\varphi = \pi$ and $\varphi = 0.98\pi$, $\varphi = -0.0785\pi$ and $\varphi = -0.0585\pi$) are shown in Figs. 1(c)–1(e), respectively. In Figs. 1(c)–1(e), there is no narrow transmission peak at the breakpoints shown in the red curve. However, when a little phase shift $\varphi = 0.02\pi$ is introduced, sharp Fano resonant peaks appear suddenly, shown in the blue curve. This is a distinctive feature near the BIC points.

We calculate the Q factor along the k_x axis at different phase differences $\varphi = 0$, $\varphi = \pm\pi$, and $\varphi = -0.0785\pi$ in Figs. 2(a)–2(c). The Q factor tends to infinity from the BIC points. The transverse magnetic (TM_1 and TM_2) band structures of our corrugated structure are shown in Figs. 2(d) and 2(f), and the insets show magnetic field profiles (y component) at the Γ point, respectively. More importantly, we discuss the coupling between TM_1 and TM_2 modes. When the phase difference is $\pm\pi$, the structure has C_2 and up-down mirror symmetry, and odd (TM_1) and even (TM_2) modes cannot couple because they are orthogonal in the symmetric structure, as shown in Fig. 2(e). When the mirror symmetry is broken, the odd and even modes will couple and generate eigenmodes with rich dispersion properties [Figs. 2(d) and 2(f)].

In order to obtain the clear influence of the phase difference on BICs, we select a horizontal plane above and below the structure, with the distribution of far-field polarization states (left) and phase (right) in upward [Figs. 3(a) and 3(b) and the top panel of Fig. 3(c), where Figs. 3(a) and 3(b) have the same upward and downward polarization states and polarization orientation angle maps due to symmetry of the structure] and downward [bottom panel of Fig. 3(c)] radiation. From Fig. 3 we find that all the BICs are vortex centers in the polarization vector of the far-field radiation, which can be described by a topological charge q,

$$q = \frac{1}{2\pi}\oint_L d\mathbf{k}_\parallel \cdot \nabla_k \theta(\mathbf{k}_\parallel), \qquad (1)$$

where $\mathbf{k}_\parallel$ is the in-plane wave vector, $\theta(\mathbf{k}) = \frac{1}{2}\arg[S_1(\mathbf{k}) + iS_2(\mathbf{k})]$ is the argument of the polarization vector of far-field radiation projected into the x-y plane, and L is a closed path that goes counterclockwise around the polarization singularity [33,65]. $S_i(\mathbf{k}_\parallel)$ is the Stokes parameter.

The topological charges of all breakpoints obtained by using Eq. (1) are labeled in Fig. 3. The polarization orientation angle maps of the projection of far-field radiation in an x-y plane above (top panel) or below (bottom panel) the structure are given in Fig. 3. From the polarization orientation angle maps, we can determine easily the topological charges of each V point. We can see that the Q factor becomes infinite at all the breakpoints. When the phase difference is $\varphi = 0$ and $\varphi = \pm\pi$, the polarization state distribution associated with points A and B is shown in Figs. 3(a) and 3(b). For a phase difference $\varphi = -0.0785\pi$, it can be dynamically manipulated via shifting of the phase difference without breaking the P symmetry of the structure. We find two V points in the polarization state distribution of upward (downward) radiation [Fig. 3(c)]. The two V points at the Γ point correspond to BIC and have infinite Q factors, however, the Q factor of V points at $k_x a/2\pi = \mp 0.0111$ is finite, which means the existence of radiation there. From Fig. 3(c) we can see the Q factor of the V points at $k_x a/(2\pi) = \mp 0.0111$ is much less than that of BIC points, which implies the existence of far-field radiation.

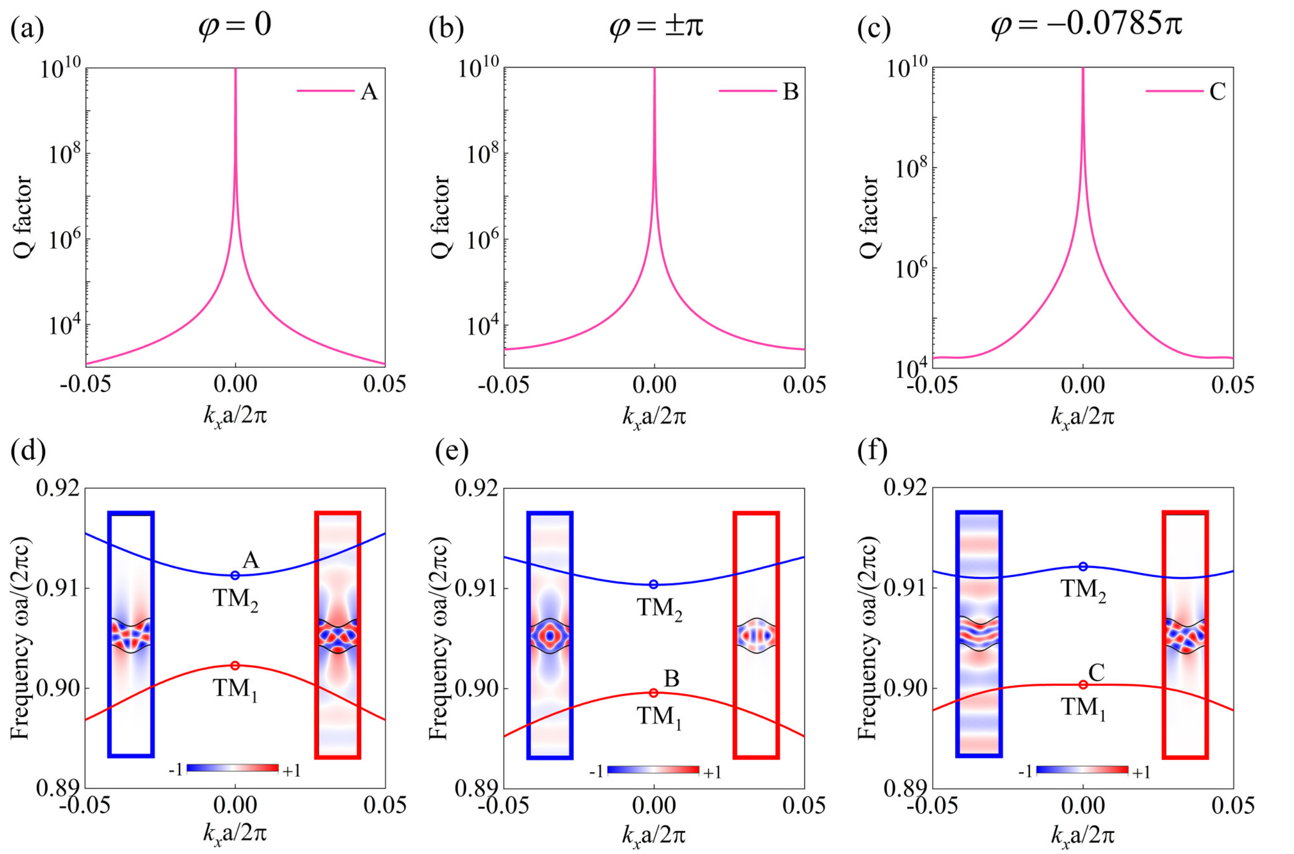

FIG. 2. (a)–(c) The Q factor along the k_x axis at the BIC points, and (d)–(f) the calculated band structures along the k_x axis for various phase differences $\varphi = 0$, $\varphi = \pm\pi$ and $\varphi = -0.0785\pi$. The right and left insets show the magnetic field profile (y component) of the TM_1 and TM_2 bands at the Γ point, respectively.

In order to reveal the radiation properties for $\varphi = -0.0785\pi$, we give more details about the polarization vector distribution of far-field, radiation loss, magnetic field profiles, and polarization orientation angle maps in Fig. 4. The corresponding upward and downward radiation losses are given in Fig. 4(a). For the V point P, the upward radiation loss tends to zero, which means the upward radiation is almost forbidden. The downward radiation loss tends to be a finite value, which means that there is a downward radiation. Similarly, the V point Q corresponds to an upward radiation. Our analysis is reconfirmed by the magnetic (y component) distributions [Fig. 4(b)], in which we can find an obvious downward radiation at $k_x a/(2\pi) = -0.0111$ (P point) and an upward radiation at $k_x a/(2\pi) = 0.0111$ (Q point), indicating that two UGRs generate. In contrast, a pair of V points blocks both upward and downward radiation, and the Γ point $[k_x a/(2\pi) = 0]$ becomes a BIC. Therefore, we obtain the BIC at the Γ point and the UGRs at $k_x a/(2\pi) = \mp 0.0111$ simultaneously, which implies the coexistence of BIC and UGRs is realized when $\varphi = -0.0785\pi$ in momentum space. Different from previous studies where the evolution between BICs and UGRs is achieved via adjusting the structure parameters, we can achieve the light controlling from the BICs to UGRs under a specified phase difference without changing the structure parameters.

In addition, the radiation loss can be controlled by changing the phase difference. When $\varphi = -0.0805\pi$, two V points of UGRs with upward and downward radiation move far away from each other, as shown in Fig. 4(c). At the same time the V points associated with BICs shift too, which results in the vanishing of BIC at the Γ point. From the polarization state distribution in Fig. 4(d), we can see four V points in the upward and downward radiation. Due to the moving of the V points, the BIC point turns into two UGR points, while the Q factor is no longer infinite. The continuous changing of the phase difference simultaneously generates four V points after breaking the C_2 symmetry of the structure. From Fig. 4 we find that BICs (UGRs) are due to the presence of V points blocking the upward and downward (upward or downward) radiation channels. The V points can be moved by adjusting the phase difference. When only one radiation channel is suppressed the UGR is generated, and when upward and downward radiation channels are suppressed the BIC is achieved.

In Fig. 4(e) we give the comparison of the Q factor for $\varphi = -0.0785\pi$ and $\varphi = -0.0805\pi$. The magenta line shows the BIC at the Γ point leads to the infinite Q factor when $\varphi = -0.0785\pi$. Interestingly, for $\varphi = -0.0805\pi$ the BIC turns into UGRs, and the superposition of four UGRs (V points) leads to the generation of a high Q factor platform as shown by the green curve. The polarization orientation angle maps of the projection of upward (top panel) and downward (bottom panel) radiation when $\varphi = -0.0805\pi$ are shown in Fig. 4(f). From the polarization orientation angle maps, the V points and their topological charge can be obtained clearly. The total

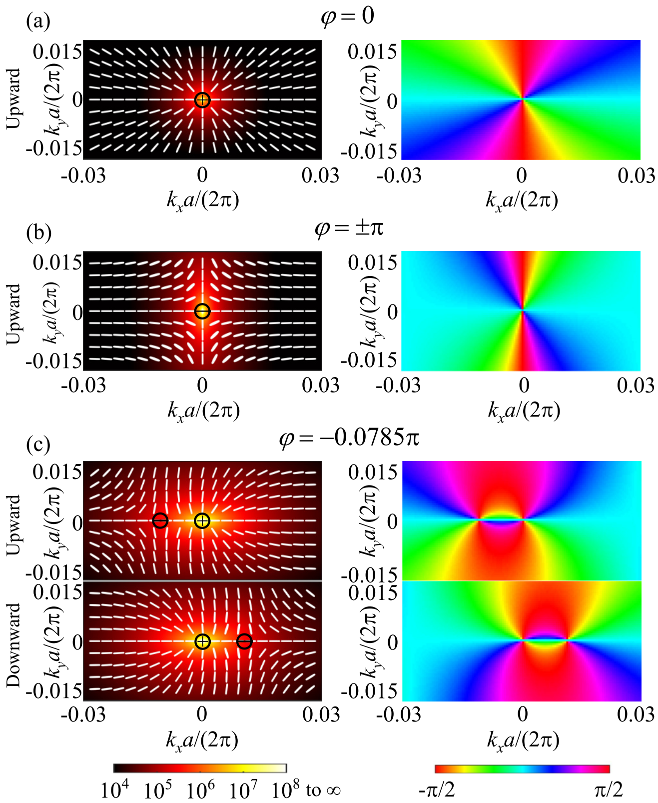

FIG. 3. The far-field polarization states and Q factor distribution (left), and polarization orientation angle maps (right) of the upward and downward. The Q factor is shown as the background color. The phase difference between the upper and lower surfaces is chosen as (a) $\varphi = 0$, (b) $\varphi = \pm\pi$, (c) $\varphi = -0.0785\pi$.

topological charge remains compared with $\varphi = -0.0785\pi$. The realization of a high Q factor platform and the coexistence of BICs and UGRs have important significance for manipulating light radiation.

Conclusion. In conclusion, BIC points are supported in a corrugated structure whose symmetry can be controlled through adjusting the phase differences between the upper and lower surfaces. When the up-down mirror symmetry is broken the odd and even modes will couple, which results in the coexistence of BICs and UGRs at a specified phase difference. The phase difference can lead to the moving of V points, and the rearrangement of the four V points results in the generation of a high Q factor platform. Our findings offer a unique approach to manipulating far-field radiation including different radiative channels and high Q factors of resonances, for potential applications in sharp spectral filters, optical vortex generators, and the enhancement of nonlinearity.

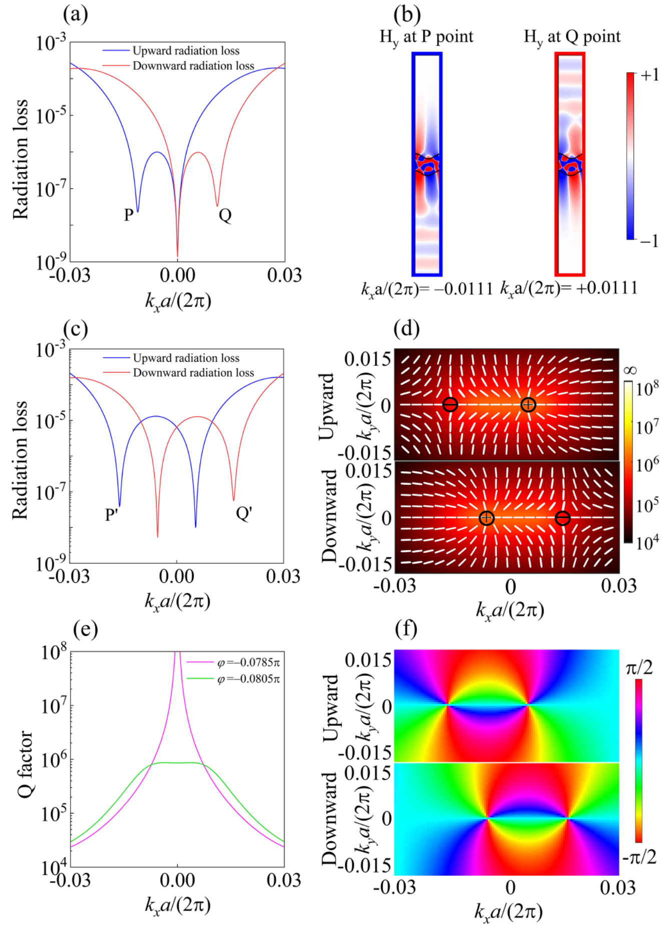

FIG. 4. Radiation properties of the dielectric corrugated grating with phase difference $\varphi = -0.0785\pi$ and $\varphi = -0.0805\pi$. (a) Radiation losses along the k_x axis of the structure with $\varphi = -0.0785\pi$. (b) The magnetic field profiles (y component) of eigenmodes at $k_xa/(2\pi) = -0.0111$ and $k_xa/(2\pi) = 0.0111$ (P and Q points). (c) Radiation losses along the k_x axis of the structure with $\varphi = -0.0805\pi$. (d) The far-field polarization states of upward and downward radiation with $\varphi = -0.0805\pi$. (e) Comparison of Q factors. (f) The polarization orientation angle maps of upward and downward radiation with $\varphi = -0.0805\pi$.

Acknowledgment. The authors acknowledge the National Natural Science Foundation of China, the Program for Innovation Research of Science in Harbin Institute of Technology, and the Fundamental Research Funds for the Central Universities.

[1] C. W. Hsu, B. Zhen, A. D. Stone, J. D. Joannopoulos, and M. Soljacic, Bound states in the continuum, Nat. Rev. Mater. **1**, 16048 (2016).
[2] M. Minkov, I. A. D. Williamson, M. Xiao, and S. H. Fan, Zero-index bound states in the continuum, Phys. Rev. Lett. **121**, 263901 (2018).
[3] M. Lawrence, D. R. Barton III, J. Dixon, J. H. Song, J. van de Groep, M. L. Brongersma, and J. A. Dionne, High quality factor phase gradient metasurfaces, Nat. Nanotechnol. **15**, 956 (2020).
[4] K. Koshelev, S. Lepeshov, M. K. Liu, A. Bogdanov, and Y. Kivshar, Asymmetric metasurfaces with high-Q resonances

governed by bound states in the continuum, Phys. Rev. Lett. **121**, 193903 (2018).
[5] M. Kang, L. Mao, S. P. Zhang, M. Xiao, H. X. Xu, and C. T. Chan, Merging bound states in the continuum by harnessing higher-order topological charges, Light: Sci. Appl. **11**, 228 (2022).
[6] W. M. Ye, Y. Gao, and J. L. Liu, Singular points of polarizations in the momentum space of photonic crystal slabs, Phys. Rev. Lett. **124**, 153904 (2020).
[7] S. Mohamed, J. Wang, H. Rekola, J. Heikkinen, B. Asamoah, L. Shi, and T. K. Hakala, Controlling topology and polarization state of lasing photonic bound states in continuum, Laser Photonics Rev. **16**, 2100574 (2022).
[8] G. J. Tang, X. T. He, F. L. Shi, J. W. Liu, X. D. Chen, and J. W. Dong, Topological photonic crystals: Physics, designs, and applications, Laser Photonics Rev. **16**, 2100300 (2022).
[9] G. C. Sun, Y. Wang, Y. H. Li, Z. J. Cui, W. S. Chen, and K. Zhang, Tailoring topological nature of merging bound states in the continuum by manipulating structure symmetry of the all-dielectric metasurface, Phys. Rev. B **109**, 035406 (2024).
[10] H. Q. Luo, L. L. Liu, Z. Xi, Y. H. Lu, and P. Wang, Dynamics of diverse polarization singularities in momentum space with far-field interference, Phys. Rev. A **107**, 013504 (2023).
[11] A. Epishin, S. Reich, and E. B. Barros, Theory of plasmon-polaritons in binary metallic supercrystals, Phys. Rev. B **107**, 235122 (2023).
[12] T. Yoda and M. Notomi, Generation and annihilation of topologically protected bound states in the continuum and circularly polarized states by symmetry breaking, Phys. Rev. Lett. **125**, 053902 (2020).
[13] Q. J. Zhou, Y. Y. Fu, J. Q. Liu, H. M. Yan, H. Y. Chen, L. Gao, J. H. Jiang, and Y. D. Xu, Plasmonic bound states in the continuum in compact nanostructures, Adv. Opt. Mater. **10**, 2201590 (2022).
[14] S. Q. Li, C. H. Du, L. Z. Yin, Z. C. Gao, and F. H. Li, Quasi-bound states in the continuum of localized spoof surface plasmons, ACS Photonics **9**, 3333 (2022).
[15] J. Gu, B. Chakraborty, M. Khatoniar, and V. M. Menon, A room-temperature polariton light-emitting diode based on monolayer WS_2, Nat. Nanotechnol. **14**, 1024 (2019).
[16] A. Leitis, A. Tittl, M. K. Liu, B. H. Lee, M. B. Gu, Y. S. Kivshar, and H. Altug, Angle-multiplexed all-dielectric metasurfaces for broadband molecular fingerprint retrieval, Sci. Adv. **5**, eaaw2871 (2019).
[17] X. E. Chen, Y. Zhang, G. X. Cai, J. L. Zhuo, K. Z. Lai, and L. F. Ye, All-dielectric metasurfaces with high Q-factor Fano resonances enabling multi-scenario sensing, Nanophotonics **11**, 4537 (2022).
[18] M. K. Kroychuk, A. S. Shorokhov, D. F. Yagudin, D. A. Shilkin, D. A. Smirnova, I. Volkovskaya, M. R. Shcherbakov, G. Shvets, and A. A. Fedyanin, Enhanced nonlinear light generation in oligomers of silicon nanoparticles under vector beam illumination, Nano Lett. **20**, 3471 (2020).
[19] Z. J. Liu, Y. Xu, Y. Lin, J. Xiang, T. H. Feng, Q. T. Cao, J. T. Li, S. Lan, and J. Liu, High-Q quasibound states in the continuum for nonlinear metasurfaces, Phys. Rev. Lett. **123**, 253901 (2019).
[20] B. Real and R. A. Vicencio, Controlled mobility of compact discrete solitons in nonlinear Lieb photonic lattices, Phys. Rev. A **98**, 053845 (2018).
[21] L. Carletti, K. Koshelev, C. De Angelis, and Y. Kivshar, Giant nonlinear response at the nanoscale driven by bound states in the continuum, Phys. Rev. Lett. **121**, 033903 (2018).
[22] S. Fan and J. D. Joannopoulos, Analysis of guided resonances in photonic crystal slabs, Phys. Rev. B **65**, 235112 (2002).
[23] Y. Plotnik, O. Peleg, F. Dreisow, M. Heinrich, S. Nolte, A. Szameit, and M. Segev, Experimental observation of optical bound states in the continuum, Phys. Rev. Lett. **107**, 183901 (2011).
[24] J. Lee, B. Zhen, S.-L. Chua, W. Qiu, J. D. Joannopoulos, M. Soljačić, and O. Shapira, Observation and differentiation of unique high-Q optical resonances near zero wave vector in macroscopic photonic crystal slabs, Phys. Rev. Lett. **109**, 067401 (2012).
[25] Q. J. Song, J. S. Hu, S. W. Dai, C. X. Zheng, D. Z. Han, J. Zi, Z. Q. Zhang, and C. T. Chan, Coexistence of a new type of bound state in the continuum and a lasing threshold mode induced by PT symmetry, Sci. Adv. **6**, eabc1160 (2020).
[26] M. V. Rybin, K. L. Koshelev, Z. F. Sadrieva, K. B. Samusev, A. A. Bogdanov, M. F. Limonov, and Y. S. Kivshar, High-Q supercavity modes in subwavelength dielectric resonators, Phys. Rev. Lett. **119**, 243901 (2017).
[27] A. Cerjan, C. W. Hsu, and M. C. Rechtsman, Bound states in the continuum through environmental design, Phys. Rev. Lett. **123**, 023902 (2019).
[28] J. Jin, X. Yin, L. Ni, M. Soljačić, B. Zhen, and C. Peng, Topologically enabled ultrahigh-Q guided resonances robust to out-of-plane scattering, Nature (London) **574**, 501 (2019).
[29] X. Yin, J. Jin, M. Soljačić, C. Peng, and B. Zhen, Observation of topologically enabled unidirectional guided resonances, Nature (London) **580**, 467 (2020).
[30] M. Kang, S. Zhang, M. Xiao, and H. Xu, Merging bound states in the continuum at off-high symmetry points, Phys. Rev. Lett. **126**, 117402 (2021).
[31] Y. X. Zeng, G. W. Hu, K. P. Liu, Z. X. Tang, and C. W. Qiu, Dynamics of topological polarization singularity in momentum space, Phys. Rev. Lett. **127**, 176101 (2021).
[32] C. Zhao, W. J. Chen, J. X. Wei, W. J. Deng, Y. Z. Yan, Y. Z. Zhang, and C. W. Qiu, Electrically tunable and robust bound states in the continuum enabled by 2D transition metal dichalcogenide, Adv. Opt. Mater. **10**, 2201634 (2022).
[33] B. Zhen, C. W. Hsu, L. Lu, A. D. Stone, and M. Soljacic, Topological nature of optical bound states in the continuum, Phys. Rev. Lett. **113**, 257401 (2014).
[34] S. G. Lee, S. H. Kim, and C. S. Kee, Bound states in the continuum (BIC) accompanied by avoided crossings in leaky-mode photonic lattices, Nanophotonics **9**, 4373 (2020).
[35] X. W. Gao, C. W. Hsu, B. Zhen, X. Lin, J. D. Joannopoulos, M. Soljacic, and H. S. Chen, Formation mechanism of guided resonances and bound states in the continuum in photonic crystal slabs, Sci. Rep. **6**, 31908 (2016).
[36] S. Dai, L. Liu, D. Han, and J. Zi, From topologically protected coherent perfect reflection to bound states in the continuum, Phys. Rev. B **98**, 081405(R) (2018).
[37] J. Wang, J. Liu, S. H. Li, Y. F. Zhao, J. Du, and L. Zhu, Orbital angular momentum and beyond in free-space optical communications, Nanophotonics **11**, 645 (2022).
[38] K. D. Wang, C. Y. Guan, S. Wan, T. L. Cheng, J. H. Shi, and J. L. Liu, Observing tunable evolutions of optical singularities by C_2 symmetry breaking, Phys. Rev. B **108**, 165305 (2023).

[39] W. Z. Liu, B. Wang, Y. W. Zhang, J. J. Wang, M. X. Zhao, F. Guan, X. H. Liu, L. Shi, and J. Zi, Circularly polarized states spawning from bound states in the continuum, Phys. Rev. Lett. **123**, 116104 (2019).
[40] H. Y. Qin, Z. P. Su, M. Q. Liu, Y. X. Zeng, M. C. Tang, M. Y. Li, Y. Z. Shi, W. Huang, C. W. Qiu, and Q. H. Song, Arbitrarily polarized bound states in the continuum with twisted photonic crystal slabs, Light: Sci. Appl. **12**, 66 (2023).
[41] M. Minkov, D. Gerace, and S. H. Fan, Doubly resonant χ^2 nonlinear photonic crystal cavity based on a bound state in the continuum, Optica **6**, 1039 (2019).
[42] Y. Zhou, M. Luo, X. Y. Zhao, Y. X. Li, Q. Wang, Z. R. Liu, J. H. Guo, Z. H. Guo, J. J. Liu, and X. Wu, Asymmetric tetramer metasurface sensor governed by quasi-bound states in the continuum, Nanophotonics **12**, 1295 (2023).
[43] X. F. Yin and C. Peng, Manipulating light radiation from a topological perspective, Photonics Res. **8**, B25 (2020).
[44] J. N. Yang, S. S. Shi, S. Yan, R. Zhu, X. M. Zhao, Y. Qin, B. W. Fu, X. Q. Chen, H. C. Li, Z. C. Zuo, K. J. Jin, Q. H. Gong, and X. L. Xu, Non-orthogonal cavity modes near exceptional points in the far field, Commun. Phys. **7**, 13 (2024).
[45] J. K. Nayak, H. Suchiang, S. K. Ray, S. Guchhait, A. Banerjee, S. D. Gupta, and N. Ghosh, Spin-direction-spin coupling of quasiguided modes in plasmonic crystals, Phys. Rev. Lett. **131**, 193803 (2023).
[46] Q. K. Liu, Y. Li, Z. D. Lu, Y. J. Zhou, W. M. Liu, X. Q. Luo, and X. L. Wang, Steerable chiral optical responses unraveled in planar metasurfaces via bound states in the continuum, Phys. Rev. B **108**, 155410 (2023).
[47] Q. Jiang, P. Hu, J. Wang, D. Z. Han, and J. Zi, General bound states in the continuum in momentum space, Phys. Rev. Lett. **131**, 013801 (2023).
[48] Q. Liu, L. Qu, Z. D. Gu, D. Zhang, W. Wu, W. Cai, M. X. Ren, and J. J. Xu, Boosting second harmonic generation by merging bound states in the continuum, Phys. Rev. B **107**, 245408 (2023).
[49] K. L. Koshelev, Z. F. Sadrieva, A. A. Shcherbakov, Y. S. Kivshar, and A. A. Bogdanov, Bound states in the continuum in photonic structures, Phys. Usp. **66**, 494 (2023).
[50] S. J. You, M. M. Zhou, L. Xu, D. L. Chen, M. H. Fan, J. Huang, W. B. Ma, S. Y. Luo, M. Rahmani, C. B. Zhou, A. E. Miroshnichenko, and L. J. Huang, Quasi-bound states in the continuum with a stable resonance wavelength in dimer dielectric metasurfaces, Nanophotonics **12**, 2051 (2023).
[51] Z. Chen, X. Yin, J. Jin, Z. Zheng, Z. Zhang, F. Wang, L. He, B. Zhen, and C. Peng, Observation of miniaturized bound states in the continuum with ultra-high quality factors, Sci. Bull. **67**, 359 (2022).
[52] S. Mukherjee, A. Spracklen, D. Choudhury, N. Goldman, P. Öhberg, E. Andersson, and R. R. Thomson, Observation of a localized flat-band state in a photonic Lieb lattice, Phys. Rev. Lett. **114**, 245504 (2015).
[53] Z. G. Dong, Z. Mahfoud, R. Paniagua-Domínguez, H. T. Wang, A. I. Fernández-Domínguez, S. Gorelik, S. T. Ha, F. Tjiptoharsono, A. I. Kuznetsov, M. Bosman, and J. K. W. Yang, Nanoscale mapping of optically inaccessible bound-states-in-the-continuum, Light: Sci. Appl. **11**, 20 (2022).
[54] W. Wang, X. L. Wang, and G. C. Ma, Extended state in a localized continuum, Phys. Rev. Lett. **129**, 264301 (2022).
[55] A. Abdrabou, L. J. Yuan, W. T. Lu, and Y. Y. Lu, Parametric dependence of bound states in the continuum: A general theory, Phys. Rev. A **107**, 033511 (2023).
[56] J. W. You, Z. H. Lan, Q. Ma, Z. Gao, Y. H. Yang, F. Gao, M. Xiao, and T. J. Cui, Topological metasurface: From passive toward active and beyond, Photonics Res. **11**, B65 (2023).
[57] D. C. Marinica, A. G. Borisov, and S. V. Shabanov, Bound states in the continuum in photonics, Phys. Rev. Lett. **100**, 183902 (2008).
[58] C. L. Zou, J. M. Cui, F. W. Sun, X. Xiong, X. B. Zou, Z. F. Han, and G. C. Guo, Guiding light through optical bound states in the continuum for ultrahigh-Q microresonators, Laser Photonics Rev. **9**, 114 (2015).
[59] J. J. Wang, L. Shi, and J. Zi, Spin Hall effect of light via momentum-space topological vortices around bound states in the continuum, Phys. Rev. Lett. **129**, 236101 (2022).
[60] Y. Chen, H. C. Deng, X. B. Sha, W. J. Chen, R. Z. Wang, Y. H. Chen, D. Wu, J. R. Chu, Y. S. Kivshar, S. M. Xiao, and C. W. Qiu, Observation of intrinsic chiral bound states in the continuum, Nature (London) **613**, 474 (2023).
[61] Y. H. Wang, Y. B. Fan, X. D. Zhang, H. J. Tang, Q. H. Song, J. C. Han, and S. M. Xiao, Highly controllable etchless perovskite microlasers based on bound states in the continuum, ACS Nano **15**, 7386 (2021).
[62] Z. Sakotic, P. Stankovic, V. Bengin, A. Krasnok, A. Alu, and N. Jankovic, Non-Hermitian control of topological scattering singularities emerging from bound states in the continuum, Laser Photonics Rev. **17**, 2200308 (2023).
[63] A. Overvig, N. F. Yu, and A. Alu, Chiral quasi-bound states in the continuum, Phys. Rev. Lett. **126**, 073001 (2021).
[64] K. Y. Lee, K. W. Yoo, S. Cheon, W. J. Joo, J. W. Yoon, and S. H. Song, Synthetic topological nodal phase in bilayer resonant gratings, Phys. Rev. Lett. **128**, 053002 (2022).
[65] Y. W. Zhang, A. Chen, W. Z. Liu, C. W. Hsu, B. Wang, F. Guan, X. H. Liu, L. Shi, L. Lu, and J. Zi, Observation of polarization vortices in momentum space, Phys. Rev. Lett. **120**, 186103 (2018).